arXiv:1601.07069v1 [cond-mat.str-el] 26 Jan 2016

# Jahn-Teller effect in systems with strong on-site spin-orbit coupling

Ekaterina M. Plotnikova,[1] Maria Daghofer,[2] Jeroen van den Brink,[1] and Krzysztof Wohlfeld[3, 4]

[1] *IFW Dresden, Helmholtzstr. 20, 01069 Dresden, Germany**
[2] *Institute for Functional Materials and Quantum Technologies, University of Stuttgart, Pfaffenwaldring 57 D-70550 Stuttgart, Germany*
[3] *Stanford University and SLAC National Accelerator Laboratory, 2575 Sand Hill Rd, Menlo Park, CA 94025 USA*
[4] *Institute of Theoretical Physics, Faculty of Physics, University of Warsaw, Pasteura 5, PL-02093 Warsaw, Poland*

(Dated: January 27, 2016)

When strong spin-orbit coupling removes orbital degeneracy, it would at the same time appear to render the Jahn-Teller mechanism ineffective. We discuss such a situation, the $t_{2g}$ manifold of iridates, and show that, while the Jahn-Teller effect does indeed not affect the $j_{\rm eff} = 1/2$ antiferromagnetically ordered ground state, it leads to distinctive signatures in the $j_{\rm eff} = 3/2$ spin-orbit exciton. It allows for a hopping of the spin-orbit exciton between the nearest neighbor sites without producing defects in the $j_{\rm eff} = 1/2$ antiferromagnet. This arises because the lattice-driven Jahn-Teller mechanism only couples to the orbital degree of freedom, but is not sensitive to the phase of the wave function that defines isospin $j_z$. This contrasts sharply with purely electronic propagation, which conserves isospin, and presence of Jahn-Teller coupling can explain some of the peculiar features of measured resonant inelastic x-ray scattering spectra of $Sr_2IrO_4$.

PACS numbers: 71.27.+a, 71.70.Ej, 75.30.Et, 75.10.Jm

*Introduction* The discovery that spin-orbit coupling (SOC) can induce bulk insulators with conducting edge states, which are symmetry protected against back scattering, has in recent years revived interest in spin-orbit coupled materials [1, 2]. While typical topological insulators are at most weakly correlated, the interplay of electron-electron interaction and spin-orbit coupling has also received enhanced attention: On one hand, the combination was soon discovered as a promising route to alternative topologically nontrivial states, from topological Mott [3, 4] over fractional Chern [5] insulators to a potential realization [6, 7] for Kitaev's celebrated spin-liquid phase with its anyonic excitations [8, 9]. On the other hand, spin-orbit coupled and correlated square-lattice iridates are emerging as a sister-system to high-$T_C$ cuprates [10–17].

The cuprate-like physics and the Kitaev-Heisenberg model supporting the spin liquid are both understood to arise as the low-energy limit in iridium compounds like square-lattice $Sr_2IrO_4$ [6, 10, 11] and honeycomb-lattice $Na_2IrO_3$ [7, 18]. In such iridates, the $t_{2g}$ levels of the $5d$ shell are almost filled, the single hole is subject to both strong SOC and appreciable correlations. The $t_{2g}$ manifold can be described as an effective angular momentum $l_{\rm eff} = 1$ and SOC locally couples spin $\mathbf{s}$ and $\mathbf{l}$ to a total angular momentum $\mathbf{j}$. The threefold orbital degeneracy of the $t_{2g}$ states is thus lifted by SOC and on-site Hubbard interaction can subsequently open a charge gap and stabilize a localized (pseudo)spin $j_{\rm eff} = 1/2$ [6, 10]. Due to the orbital part of the $j_{\rm eff} = 1/2$ wave function, couplings between these effective spins are sensitive to lattice geometry and support a variety of quantum states.

A striking difference to $3d$ systems with negligible [19] SOC is the lifting of the orbital degeneracy: a single hole (or electron) in a $3d$ shell has an orbital degree of freedom in addition to spin – as opposed to the single $j_{\rm eff} = 1/2$ degree of freedom of the $5d$ hole. As a consequence, an analogous $3d$ system can not only feature

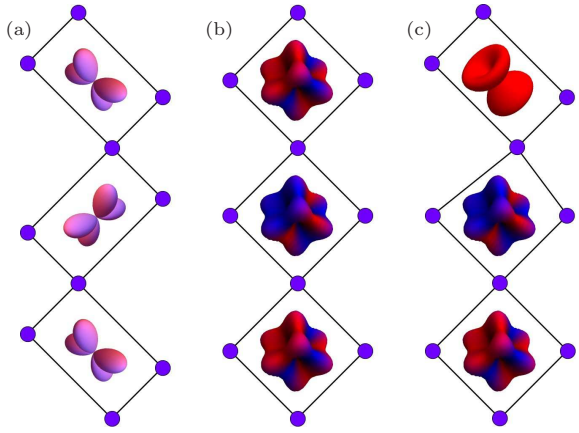


FIG. 1: Cartoon picture showing the Jahn-Teller effect in systems *without* and *with* strong SOC: (a) Weak SOC – oxygen displacements following 'conventional' Jahn-Teller effect for the ground state with e.g. the $d_{xz}/d_{yz}$ alternating orbital order. (b) Strong SOC – no oxygen displacements due to the quenched Jahn-Teller effect for the ground state with e.g. $|j_{\rm eff} = 1/2,\ j_z = 1/2\rangle/|j_{\rm eff} = 1/2,\ j_z = -1/2\rangle$ alternating spin-orbital order (antiferromagnetic order of $j_{\rm eff} = 1/2$ isospins). (c) Strong SOC – oxygen displacements around the $|j_{\rm eff} = 3/2,\ j_z = -3/2\rangle$ exciton (which 'lives' in the antiferromagnetic $j_{\rm eff} = 1/2$ ground state) showing that such a system is Jahn-Teller active.

orbital order in addition to magnetism, but the Jahn-Teller effect [cf. Fig. 1(a)] would moreover be expected to couple the orbital degree of freedom to the lattice [20–23]. In contrast, the quenching of the orbital degree of freedom by SOC removes the possibility of orbital order and would at first sight also appear to suppress Jahn-Teller effect and coupling to the lattice.

In this Letter, we are nevertheless going to discuss the impact of the Jahn-Teller effect on $5d$ systems with strong SOC: While it is indeed absent for the ground state consisting of $j_{\rm eff}=1/2$ pseudospins, see Fig. 1(b), we are going to show that it leaves clear signatures in the dynamics of collective *excitations* into the $j_{\rm eff}=3/2$ sector (i.e. excitons). As seen in Fig. 1(c), the Jahn-Teller effect is here not quenched and can allow for a novel type of excitonic propagation. In particular, we propose that the experimentally observed branch of the exciton dispersion with the minimum at the $\Gamma$ point [14], which can not be explained using superexchange alone, finds a natural explanation within the present Jahn-Teller model.

*Finite Jahn-Teller for excited states* Since the SOC constant $\lambda>0$ is assumed to be the largest energy scale involved, with $\lambda=0.382$ eV in $Sr_2IrO_4$ [14], we start our analysis by diagonalizing this dominant term. This is achieved by a basis change from $\mathbf{s}$ (the $s=1/2$ spin) and $\mathbf{l}$ (the effective $l_{\rm eff}=1$ orbital moment) to total angular momentum $\mathbf{j}=\mathbf{l}+\mathbf{s}$. For a single hole in the $t_{2g}$ shell, SOC interaction $\mathcal{H}_{\rm SOC}=\lambda\sum_i \mathbf{l}_i\cdot\mathbf{s}_i$ becomes then $\mathcal{H}_{\rm SOC}=\lambda/2\sum_i(\mathbf{j}_j^2-\mathbf{s}_j^2-\mathbf{l}_j^2)$ and the ground state is given by the doubly-degenerate $j_{\rm eff}=1/2$ manifold, while the $j_{\rm eff}=3/2$ manifold forms the excited states at energy $3\lambda/2$. (A crystal-field splitting $\Delta$ can explicitly be included into this analysis [6, 24], but is omitted here for clarity)

For $t_{2_g}$ electrons, the orbital operators $\mathbf{l}$ couple both to the tetragonal phonon modes $Q_2$ and $Q_3$ (the $e_g$ modes) and to trigonal phonon modes $Q_4$, $Q_5$, and $Q_6$ (the $t_{2g}$ modes). After integrating out the phonons, the Jahn-Teller interaction is expressed in terms of $\mathbf{l}$ [21]:

$$\begin{aligned}\mathcal{H}_{\rm JT}=&V\sum_{\langle\mathbf{i},\mathbf{j}\rangle}\left[\left(l_{\mathbf{i}}^z\right)^2-\frac{2}{3}\right]\left[\left(l_{\mathbf{j}}^z\right)^2-\frac{2}{3}\right]\\&+V\sum_{\langle\mathbf{i},\mathbf{j}\rangle}\left[\left(l_{\mathbf{i}}^x\right)^2-\left(l_{\mathbf{i}}^y\right)^2\right]\left[\left(l_{\mathbf{j}}^x\right)^2-\left(l_{\mathbf{j}}^y\right)^2\right]\\&+\kappa V\sum_{\langle\mathbf{i},\mathbf{j}\rangle}\left[\left(l_{\mathbf{i}}^x l_{\mathbf{i}}^y+l_{\mathbf{i}}^y l_{\mathbf{i}}^x\right)\left(l_{\mathbf{j}}^x l_{\mathbf{j}}^y+l_{\mathbf{j}}^y l_{\mathbf{j}}^x\right)+...\right].\end{aligned}\tag{1}$$

The two classes of phonon modes lead to two *a priori* independent Jahn-Teller coupling constants $V_{e_g}\equiv V$ and $V_{t_{2g}}\equiv\kappa V$; as $V_{t_{2g}}$ is typically much smaller than $V_{e_g}$, we set $\kappa=0.1$. The Jahn-Teller interaction scale $V$ can from experiment [25] be inferred to be non-negligible, but as its strength is at present unclear, we leave it as a free parameter.

The Jahn-Teller term $H_{\rm JT}$ is now, via straightforward but tedious calculations, transformed into the eigenbasis of $\mathcal{H}_{\rm SOC}$, i.e., written in terms of $j$ states:

$$\mathcal{H}_{\rm JT}=\mathcal{H}_{\rm JT}(1/2,1/2)+\mathcal{H}_{\rm JT}(3/2,1/2)+\mathcal{H}_{\rm JT}(3/2,3/2).\tag{2}$$

The first term $\mathcal{H}_{\rm JT}(1/2,1/2)$ denotes the Jahn-Teller interaction between two $j_{\rm eff}=1/2$ states – it vanishes as expected, reflecting the quenching of orbital physics within the $j_{\rm eff}=1/2$ subshell. The last term $\mathcal{H}_{\rm JT}(3/2,3/2)$ between two $j_{\rm eff}=3/2$ states can only contribute if a large number of $j_{\rm eff}=3/2$ states are present and is thus strongly suppressed at large $\lambda$. The term $\mathcal{H}_{\rm JT}(3/2,1/2)$ describes the interaction between one $j_{\rm eff}=1/2$ and one $j_{\rm eff}=3/2$ site: Even at strong SOC, this term becomes relevant when an (iso)orbital excitation raises a single hole into a $j_{\rm eff}=3/2$ state [13, 14].

*Model* The $j_{\rm eff}=3/2$ excitation, an exciton, can be created in resonant inelastic X-ray scattering (RIXS) and has been discussed in two recent theoretical and experimental studies [13, 14]. It is described by the Green function

$$G(\mathbf{k},\omega)=Tr\langle 0|\hat{\chi}_{\mathbf{k}}\frac{1}{\omega-H+i\delta}\hat{\chi}_{\mathbf{k}}^\dagger|0\rangle,\tag{3}$$

where the $\hat{\chi}_{\mathbf{k}}^\dagger$ is a vector of four creation operators that create an exciton with momentum $\mathbf{k}$ and isospin quantum number $j_z=\pm1/2,\pm3/2$. The Hamiltonian $H$ describes the dynamics of the exciton coupling to a background of $j_{\rm eff}=1/2$ isospins, a minimal Hamiltonian is

$$H=H_{\rm SE}^{\rm mag}+H_{\rm SE}^{\rm exc}+H_{\rm JT}^{\rm exc}\ .\tag{4}$$

The first term $H_{\rm SE}^{\rm mag}$ is the superexchange interaction between $j_{\rm eff}=1/2$ isospins, where we include up to third-neighbor processes $\propto\{J_1,J_2,J_3\}$ [see Eq. (6) of the supplemental materials of Ref. [14]]. It stabilizes an alternating order of $j_{\rm eff}=1/2$ isospins with magnon-like excitations [13, 14]. The terms $H_{\rm SE}^{\rm exc}$ and $H_{\rm JT}^{\rm exc}=\mathcal{H}_{\rm JT}(3/2,1/2)$ describe superexchange and Jahn-Teller interaction between one $j_{\rm eff}=1/2$ and one $j_{\rm eff}=3/2$ site, these terms allow the exciton to move.

Without the Jahn-Teller–mediated motion, i.e. for $H=H_{\rm SE}^{\rm mag}+H_{\rm SE}^{\rm exc}$, the problem was discussed in Refs. 13, 14. Exciton propagation due to superexchange is analogous to the mechanism governing orbital excitations in cuprates [26, 27] and is strongly coupled to the magnon-like $j_{\rm eff}=1/2$ excitations. We are going to show here that the Jahn-Teller coupling $\mathcal{H}_{\rm JT}(3/2,1/2)$ provides an additional channel for delocalization whose signatures can be clearly distinguished from the pure superexchange scenario.

Following Refs. [13, 14], we extend a scheme that was widely used to describe motion in an antiferromagnetic background [28–31] in order to include Jahn-Teller–mediated exciton motion. The scheme amounts

to applying Holstein-Primakoff, Fourier and Bogoliubov transformations (see Ref. [32] for details) to arrive at the Hamiltonian

$$H_{\rm SE}^{\rm mag} = \sum_{\mathbf{k}} \omega_{\mathbf{k}} a_{\mathbf{k}}^\dagger a_{\mathbf{k}}, \tag{5}$$

$$H_{\rm SE}^{\rm exc} + H_{\rm JT}^{\rm exc} = \sum_{\mathbf{k}} (\hat{E}_{\mathbf{k}}^{\rm SE} + \hat{E}_{\mathbf{k}}^{\rm JT}) \hat{\chi}_{\mathbf{k}}^\dagger \hat{\chi}_{\mathbf{k}} \tag{6}$$

$$+ \sum_{\mathbf{k},\mathbf{q}} \left[ (\hat{M}_{\mathbf{k},\mathbf{q}}^{\rm SE} + \hat{M}_{\mathbf{k},\mathbf{q}}^{\rm JT}) \hat{\chi}_{\mathbf{k}}^\dagger \hat{\chi}_{\mathbf{k}-\mathbf{q}} a_{\mathbf{q}} + h.c. \right]. \tag{7}$$

Equation (5) describes the isospin 'magnons' originating from $H_{\rm SE}^{\rm mag}$, $a_{\mathbf{k}}^\dagger$ creates a magnon with momentum $\mathbf{k}$ and energy $\omega_{\mathbf{k}}$, see Ref. [32]. A free exciton hopping is included in Eq. (6), it can either be due to second- and third-neighbor superexchange [14], or originate from coupling to the lattice. Finally, Eq. (7) captures the coupling between exciton hopping and the isospin background: Both Jahn-Teller effect and superexchange can allow the exciton to exchange place with a nearest-neighbor isospin without flipping said isospin. This creates 'faults' in the alternating order, see Fig. 4(a), and thus creates or annihilates magnons.

Let us now discuss in more detail the contributions due to the Jahn-Teller effect; for the pure superexchange problem, we refer to Refs. [13, 14]. The Jahn-Teller vertex $\hat{M}_{\mathbf{k},\mathbf{q}}^{\rm JT}$ and the free excitonic dispersion $\hat{E}_{\mathbf{k}}^{\rm JT}$ are calculated here from $\mathcal{H}_{\rm JT}(3/2, 1/2)$ and read: $\hat{M}_{\mathbf{k},\mathbf{q}}^{\rm JT} = zV\hat{m}^{\rm JT} \cdot |\gamma_{\mathbf{k}} v_{\mathbf{q}} + \gamma_{\mathbf{k}-\mathbf{q}} u_{\mathbf{q}}|/\sqrt{N}$ and $\hat{E}_{\mathbf{k}}^{\rm JT} = zV\hat{e}^{\rm JT} \cdot |\gamma_{\mathbf{k}}|$ where $N$ is the total number of sites, $z = 4$ is the coordination number for a square lattice, and $\gamma_{\mathbf{k}} = \frac{1}{2}(\cos k_x + \cos k_y)$. The Bogoliubov coefficients $u_{\mathbf{k}}, v_{\mathbf{k}}$ and the diagonal (off-diagonal) matrix $\hat{m}^{\rm JT}$ ($\hat{e}^{\rm JT}$) are explicitly given in Ref. [32]. The crucial new feature will turn out to come from the free dispersion $\hat{E}_{\mathbf{k}}^{\rm JT}$, where the Jahn-Teller effect induces a nearest-neighbor contribution absent from superexchange.

*Results* We evaluate the Green function Eq. (3) using the self-consistent Born approximation (SCBA) – a diagrammatic approach that takes into account diagrams of rainbow-type (see e.g. Ref. [28]). The excitonic spectral functions are calculated numerically for a $32 \times 32$ cluster, taking into account 'matrix elements' depending on the angle of the incident beam [14], and shown in Fig. 2. The most striking difference to the pure superexchange scenario becomes visible in the so-called 'normal' RIXS geometry [cf. Fig. 2(a)]: a dispersive feature at around 0.4 eV (denoted as A in the figure) that has its minimal energy at $\mathbf{k} = (0, 0)$ and disperses upward towards the zone boundary, where it merges with the B feature.

An unexplained feature with minimum at the Γ point was observed in normal-incidence RIXS experiments on $Sr_2IrO_4$ [14], albeit with a weaker intensity. This discrepancy may be due to (i) contributions to the RIXS intensity of the exciton beyond the one determined in the fast core-hole approximation [33, 34] or (ii) the SCBA over-emphasizing the quasiparticle spectral weight [14]. Some fine-tuning of the unknown constant $V$ is needed to reproduce the experimental dispersion, especially the merging with the B feature, see Ref. [32] for details. It is here worth noting that a similar peak was also seen in $Na_2IrO_3$ [35], where it does not merge with the higher-energy features, suggesting that the merging may be a detail specific to $Sr_2IrO_4$. In contrast and as discussed below, the minimum at the Γ point is a robust and characteristic feature of Jahn-Teller–mediated propagation, because superexchange–driven peaks invariably have a *maximum* at the Γ point.

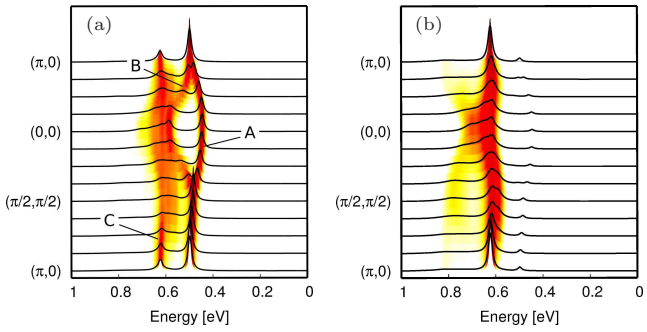


FIG. 2: Spin-orbit exciton with both superexchange and Jahn-Teller interaction, see (5) - (7) calculated using the SCBA. Intensities are given for two RIXS geometries: (a) normal and (b) grazing incidence [14]. 'A', 'B', 'C' in panel (a) denote three main features of the spectrum. Jahn-Teller interaction $V = 0.8J_1$ and broadening $\delta = 0.05J_1$. Superexchange parameters $J_2 = -0.33J_1$, $J_3 = 0.25J_1$, $W_1 = 0.5J_1$ [14], and $W_2 = W_3 = 0$. Following Ref. [14] on-site energy of the exciton is $10J_1 \approx \frac{3}{2}\lambda$, crystal-field splitting between $|j_z| = 1/2$ and $|j_z| = 3/2$ states is $2.29J_1$, and $J_1 = 0.06$ eV.

*Discussion* Figure 3 illustrates the qualitative difference between Jahn-Teller and superexchange mediated exciton propagation, with panels (a) and (c) showing the purely Jahn-Teller ($H_{\rm SE}^{\rm exc} \equiv 0$) and purely superexchange ($H_{\rm JT}^{\rm exc} \equiv 0$) scenarios. A striking difference is that the two quasi-particle–like branches of the superexchange case (c) become four in the Jahn-Teller case (a) – one of which has indeed a minimum at the Γ point. We continue the analysis by noting that both mechanisms allow in principle for a 'free' dispersion without disturbing the alternating isospin order, see Eq. (6), as well as for a 'polaronic' propagation involving magnons, see Eq. (7). Panels (b) and (d) include only the latter and reveal that the two mechanisms are then almost indistinguishable. This points to a dominant role for isospin fluctuations (on the scale of $J$ in both scenarios) in the 'polaronic' part of exciton motion.

This brings us to the following question: is the difference between the free dispersion relation in the superexchange and in the Jahn-Teller generic or it is just

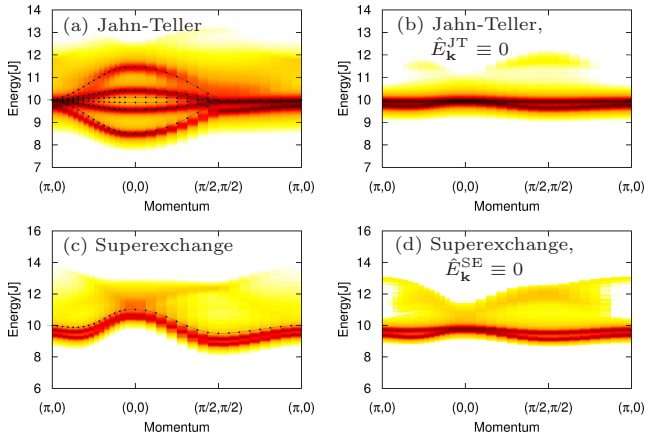


FIG. 3: Spin-orbit exciton spectra with propagation driven by either superexchange *or* Jahn-Teller interaction [calculated using SCBA, see text]: (a) Jahn-Teller only, (b) Jahn-Teller only *and* setting $\hat{E}^{\rm JT}_{\mathbf{k}} \equiv 0$, (c) superexchange only, (d) superexchange only *and* setting $\hat{E}^{\rm SE}_{\mathbf{k}} \equiv 0$. For clarity, parameters are chosen slightly different from those used in Fig. 2: $J_2 = -0.33J_1$, $J_3 = 0.25J_1$, $W_1 = 0.5J_1$, $W_2 = W_3 = 0.13J_1$ [14], Jahn-Teller interaction $V = J_1$ and broadening $\delta = 0.05J_1$. Spectra are offset by the exciton energy of $10J_1 \approx \frac{3}{2}\lambda$. Dotted lines in (a) and (c) follow the free dispersion relations given by $\hat{E}^{\rm JT}_{\mathbf{k}}$ and $\hat{E}^{\rm SE}_{\mathbf{k}}$, respectively.

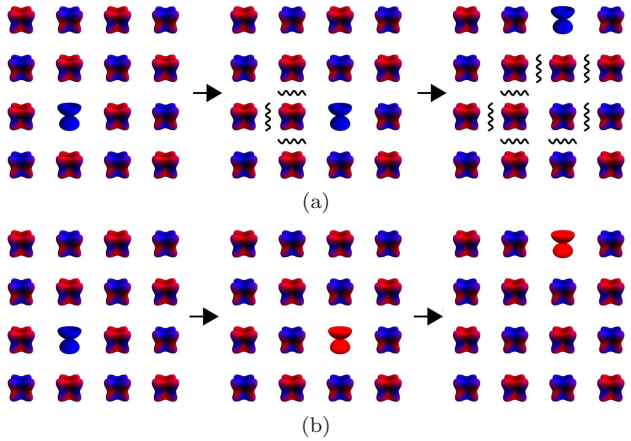


FIG. 4: Cartoon showing the two types of nearest neighbor hopping of a $j_{\rm eff} = 3/2$ exciton in the antiferromagnetically–ordered background: (a) Polaronic hopping (due to Jahn-Teller effect *or* superexchange): a $j_{\rm eff} = 3/2$ exciton with the $j_z = -3/2$ quantum number (left panel) does not change its $j_z$ quantum number during the hopping process to the nearest neighbor sites (middle / right panels) and thus the $j_{\rm eff} = 1/2$ magnons are created at each step of the excitonic hopping (wiggle lines on middle and right panels). (b) Free hopping (solely due to Jahn-Teller effect): a $j_{\rm eff} = 3/2$ exciton with the $j_z = -3/2$ quantum number (left panel) hops to the nearest neighbor site and acquires $j_z = 3/2$ quantum number (middle panel). Note that in this case the $j_{\rm eff} = 1/2$ magnons are *not* created in the system (middle / right panels).

a matter of fine-tuning of the parameters? It turns out that the difference between these two dispersion relations is of fundamental nature. The crucial aspect concerns the nearest-neighbor process, which is therefore depicted for superexchange and Jahn-Teller effect in Fig. 4. In superexchange, the exciton propagates by exchanging place with an isospin while both conserve their 'spin', i.e. their $j_z$ quantum number. In an alternating isospin order, where nearest neighbors are always of opposite $j_z$, this necessarily creates or removes 'defects', see Fig. 4(a), and thus magnons. The Jahn-Teller effect, in contrast, allows the exciton and the isospin to flip their quantum numbers while exchanging places and this allows for the nearest neighbor hopping of an exciton without creating magnons, i.e., a free excitonic dispersion. The origin of the difference is that the hole hopping driving superexchange conserves the $j_z$ quantum number, while the lattice-mediated Jahn-Teller effect is insensitive to the orbital phase. This allows $j_z$ to change during Jahn-Teller–driven propagation and accordingly yields four quasi-particles rather than two.

*Conclusions* We analyzed here the impact of a lattice-mediated Jahn-Teller effect in the presence of strong SOC, which quenches orbital degeneracy in the ground state. We found that the Jahn-Teller effect remains present for excited states, and in particular allows for a 'free' nearest-neighbor hopping of the spin-orbit exciton without producing defects in the alternating $j_{\rm eff} = 1/2$ ordering of the ground state. The tell-tale spectral signature is a dispersion with a minimum at the Γ point, which was observed in experiment but cannot be explained with superexchange alone [14]. Experiments on $Sr_2IrO_4$ at higher temperatures moreover reveal an active orbital degree of freedom and its coupling to the lattice [25], corroborating the relevance of Jahn-Teller physics when going beyond the ground state.

We have found spin-orbit coupling to substantially affect the interplay of Jahn-Teller effect and superexchange. In 3*d* compounds with weak spin-orbit coupling and unquenched orbital degeneracy (e.g. in manganites [36, 37]) both act on the same microscopic degree of freedom (i.e. orbitals) and in general lead to similar signatures. In the strongly spin-orbit–coupled 5*d* case, however, Jahn-Teller effect (determined purely by the orbital) and superexchange (strongly affected by spin-orbit entanglement) address different microscopic degrees of freedom. Their interplay is thus far more intricate, as is coupling between ions with and without strong spin-orbit coupling [38].

*Acknowledgments* We are grateful to A. M. Oleś and N. Bogdanov for fruitful discussions and in particular wish to thank B. J. Kim for discussion and helpful comments. The authors would all like to thank the staff of the Kavli Institute for Theoretical Physics (UCSB) for their kind hospitality. This research was supported in part by the National Science Foundation under Grant

No. NSF PHY11-25915 and the Deutsche Forschungsgemeinschaft (SFB 1143 and Emmy-Noether program) . K.W. acknowledges support from the DOE-BES Division of Materials Sciences and Engineering (DMSE) under Contract No. DE-AC02-76SF00515 (Stanford/SIMES) and from the Polish National Science Center (NCN) under Project No. 2012/04/A/ST3/00331.

## SUPPLEMENTAL MATERIALS

### A: Derivation of the polaronic Hamiltonian from the Jahn-Teller model

As discussed in the main text of the paper, the interaction between the orbital angular momenta as induced by the Jahn-Teller effect is described by the following Hamiltonian [21]:

$$\begin{aligned}\mathcal{H}_{\rm JT} = V\sum_{\langle \mathbf{i},\mathbf{j}\rangle}\left[\left(l^z_{\mathbf{i}}\right)^2-\frac{2}{3}\right]\left[\left(l^z_{\mathbf{j}}\right)^2-\frac{2}{3}\right]\\ + V\sum_{\langle \mathbf{i},\mathbf{j}\rangle}\left[\left(l^x_{\mathbf{i}}\right)^2-\left(l^y_{\mathbf{i}}\right)^2\right]\left[\left(l^x_{\mathbf{j}}\right)^2-\left(l^y_{\mathbf{j}}\right)^2\right]\\ + \kappa V\sum_{\langle \mathbf{i},\mathbf{j}\rangle}\left[\left(l^x_{\mathbf{i}}l^y_{\mathbf{i}}+l^y_{\mathbf{i}}l^x_{\mathbf{i}}\right)\left(l^x_{\mathbf{j}}l^y_{\mathbf{j}}+l^y_{\mathbf{j}}l^x_{\mathbf{j}}\right)+...\right].\end{aligned} \quad (8)$$

Here $V$ describes the Jahn-Teller interaction due to the coupling to the tetragonal modes, while $\kappa V$ stands for the coupling between the trigonal modes. $\mathbf{l}$ is the orbital angular moment operator for the $t_{2_g}$ electrons (see also main text of the paper).

In this part of the Supplemental Materials we show how to derive the polaronic Hamiltonian for the $j_{\rm eff}=3/2$ excitons from the above Jahn-Teller interaction – we perform this derivation in two steps:

*Firstly*, since we are interested here in the effective interaction between the $\mathbf{j}=\mathbf{l}+\mathbf{s}$ spin-orbital angular momenta (as induced by the Jahn-Teller effect), we rewrite the above Jahn-Teller Hamiltonian in the basis spanned by eigenvectors of $\mathbf{j}^2$ and $j_z$ (the '$\mathbf{j}$–basis'). Thus, we make a basis transformation from the '$\mathbf{l}\cdot\mathbf{s}$–basis' (with the effective $l_{\rm eff}=1$ and $s=1/2$):

$$\hat{A}=\left(|yz,\uparrow\rangle,|yz,\downarrow\rangle,|xz,\uparrow\rangle,|xz,\downarrow\rangle,|xy,\uparrow\rangle,|xy,\downarrow\rangle\right), \quad (9)$$

in which the above Jahn-Teller Hamiltonian is written into the '$\mathbf{j}$–basis' (with the effective $j_{\rm eff}=1/2$ or $j_{\rm eff}=3/2$ and appropriate $j_z$ quantum numbers):

$$\hat{J}=\left(|\frac{1}{2},\frac{1}{2}\rangle,|\frac{1}{2},\frac{-1}{2}\rangle,|\frac{3}{2},\frac{3}{2}\rangle,|\frac{3}{2},\frac{1}{2}\rangle,|\frac{3}{2},\frac{-1}{2}\rangle,|\frac{3}{2},\frac{-3}{2}\rangle\right). \quad (10)$$

using the Clebsch-Gordon coefficients:

$$\hat{J}=\begin{pmatrix} 0 & -\frac{1}{\sqrt{3}} & 0 & -\frac{i}{\sqrt{3}} & -\frac{1}{\sqrt{3}} & 0\\ -\frac{1}{\sqrt{3}} & 0 & \frac{i}{\sqrt{3}} & 0 & 0 & \frac{1}{\sqrt{3}}\\ -\frac{1}{\sqrt{2}} & 0 & -\frac{i}{\sqrt{2}} & 0 & 0 & 0\\ 0 & -\frac{1}{\sqrt{6}} & 0 & -\frac{i}{\sqrt{6}} & \sqrt{\frac{2}{3}} & 0\\ \frac{1}{\sqrt{6}} & 0 & -\frac{i}{\sqrt{6}} & 0 & 0 & \sqrt{\frac{2}{3}}\\ 0 & \frac{1}{\sqrt{2}} & 0 & -\frac{i}{\sqrt{2}} & 0 & 0 \end{pmatrix}\hat{A}. \quad (11)$$

As a result we obtain the Jahn-Teller Hamiltonian which *a priori* consists of three distinct terms

$$\mathcal{H}_{\rm JT}=\mathcal{H}_{\rm JT}(1/2,1/2)+\mathcal{H}_{\rm JT}(3/2,1/2)+\mathcal{H}_{\rm JT}(3/2,3/2), \quad (12)$$

as discussed already in detail in the main text. Since we are interested here in the dynamics of the $j_{\rm eff}=3/2$ exciton in the $j_{\rm eff}=1/2$ alternating orbital background (see main text), we present here the explicit form of only the $\mathcal{H}_{\rm JT}(3/2,1/2)$ part of the Hamiltonian:

$$\mathcal{H}_{\rm JT}(3/2,1/2)\equiv\mathcal{H}^{exc}_{\rm JT}=\mathcal{H}_1+\mathcal{H}_2+\mathcal{H}_3, \quad (13)$$

where

$$\begin{aligned}\mathcal{H}_1 = \frac{2V}{9}\sum_{\langle \mathbf{i},\mathbf{j}\rangle}\left(c^\dagger_{\mathbf{i}\uparrow}a_{\mathbf{i}\uparrow}a^\dagger_{\mathbf{j}\uparrow}c_{\mathbf{j}\uparrow}+c^\dagger_{\mathbf{i}\downarrow}a_{\mathbf{i}\downarrow}a^\dagger_{\mathbf{j}\downarrow}c_{\mathbf{j}\downarrow}+h.c.\right)\\ -\frac{2V}{9}\sum_{\langle \mathbf{i},\mathbf{j}\rangle}\left(c^\dagger_{\mathbf{i}\downarrow}a_{\mathbf{i}\downarrow}a^\dagger_{\mathbf{j}\uparrow}c_{\mathbf{j}\uparrow}+c^\dagger_{\mathbf{i}\uparrow}a_{\mathbf{i}\uparrow}a^\dagger_{\mathbf{j}\downarrow}c_{\mathbf{j}\downarrow}+h.c.\right)\\ +\kappa V\sum_{\langle \mathbf{i},\mathbf{j}\rangle}\left(c^\dagger_{\mathbf{i}\uparrow}a_{\mathbf{i}\downarrow}a^\dagger_{\mathbf{j}\downarrow}c_{\mathbf{j}\uparrow}+c^\dagger_{\mathbf{i}\downarrow}a_{\mathbf{i}\uparrow}a^\dagger_{\mathbf{j}\uparrow}c_{\mathbf{j}\downarrow}+h.c.\right),\end{aligned} \quad (14)$$

$$\begin{aligned}\mathcal{H}_2 = \frac{\kappa V}{3}\sum_{\langle \mathbf{i},\mathbf{j}\rangle}\left(f^\dagger_{\mathbf{i}\uparrow}a_{\mathbf{i}\uparrow}a^\dagger_{\mathbf{j}\uparrow}f_{\mathbf{j}\uparrow}+f^\dagger_{\mathbf{i}\downarrow}a_{\mathbf{i}\downarrow}a^\dagger_{\mathbf{j}\downarrow}f_{\mathbf{j}\downarrow}+h.c.\right)\\ +\frac{2V(1+\kappa)}{3}\sum_{\langle \mathbf{i},\mathbf{j}\rangle}\left(f^\dagger_{\mathbf{i}\downarrow}a_{\mathbf{i}\uparrow}a^\dagger_{\mathbf{j}\uparrow}f_{\mathbf{j}\downarrow}+f^\dagger_{\mathbf{i}\uparrow}a_{\mathbf{i}\downarrow}a^\dagger_{\mathbf{j}\downarrow}f_{\mathbf{j}\uparrow}+h.c.\right)\\ +\frac{2V(\kappa-1)}{3}\sum_{\langle \mathbf{i},\mathbf{j}\rangle}\left(f^\dagger_{\mathbf{i}\downarrow}a_{\mathbf{i}\uparrow}a^\dagger_{\mathbf{j}\downarrow}f_{\mathbf{j}\uparrow}+f^\dagger_{\mathbf{i}\uparrow}a_{\mathbf{i}\downarrow}a^\dagger_{\mathbf{j}\uparrow}f_{\mathbf{j}\downarrow}+h.c.\right),\end{aligned} \quad (15)$$

$$\begin{aligned}\mathcal{H}_3 = -\frac{\kappa V}{\sqrt{3}}\sum_{\langle \mathbf{i},\mathbf{j}\rangle}\left(f^\dagger_{\mathbf{i}\uparrow}a_{\mathbf{i}\uparrow}a^\dagger_{\mathbf{j}\downarrow}c_{\mathbf{j}\uparrow}+c^\dagger_{\mathbf{i}\uparrow}a_{\mathbf{i}\downarrow}a^\dagger_{\mathbf{j}\uparrow}f_{\mathbf{j}\uparrow}+h.c.\right)\\ -\frac{\kappa V}{\sqrt{3}}\sum_{\langle \mathbf{i},\mathbf{j}\rangle}\left(c^\dagger_{\mathbf{i}\downarrow}a_{\mathbf{i}\uparrow}a^\dagger_{\mathbf{j}\downarrow}f_{\mathbf{j}\downarrow}+f^\dagger_{\mathbf{i}\downarrow}a_{\mathbf{i}\downarrow}a^\dagger_{\mathbf{j}\uparrow}c_{\mathbf{j}\downarrow}+h.c.\right).\end{aligned} \quad (16)$$

Here $a^\dagger_{\mathbf{i}\sigma}$ denotes an operator creating a hole on site $\mathbf{i}$ in the doublet carrying effective total momentum $j_{\rm eff}=1/2$ and $\sigma\equiv j_z=\pm1/2$, while $c^\dagger_{\mathbf{i}\sigma}$ ($f^\dagger_{\mathbf{i}\sigma}$) are operators creating a hole on site $\mathbf{i}$ in the $j_{\rm eff}=3/2$ quartet with $\sigma\equiv j_z=\pm1/2,\pm1/2$.

*Secondly*, we map the above Hamiltonian $\mathcal{H}^{exc}_{\rm JT}$ onto a polaronic model (see main text of the paper for

the motivation). We follow Ref. [28] and perform the transformations:

(i) Since we assume that the ground state has antiferromagnetic order, we are allowed to rotate all isospins on one of the two antiferromagnetic sublattices:

$$a_{\mathbf{j}\sigma} \to a_{\mathbf{j}-\sigma} \quad c_{\mathbf{j}\sigma} \to c_{\mathbf{j}-\sigma} \quad f_{\mathbf{j}\sigma} \to f_{\mathbf{j}-\sigma}. \tag{17}$$

(ii) We introduce the magnon creation $\alpha_{\mathbf{i}}^{\dagger}$ and spin-orbit exciton creation $\chi_{\mathbf{i},\alpha}^{\dagger}$ operators (which are bosons and hard-core bosons, respectively). We perform the Holstein-Primakoff transformation and substitute:

$$c_{\mathbf{i}\uparrow}^{\dagger} b_{\mathbf{i}\uparrow} \to \chi_{\mathbf{i}B}^{\dagger}, c_{\mathbf{i}\downarrow}^{\dagger} b_{\mathbf{i}\uparrow} \to \chi_{\mathbf{i}C}^{\dagger}, \tag{18}$$

$$c_{\mathbf{i}\uparrow}^{\dagger} b_{\mathbf{i}\downarrow} \to \chi_{\mathbf{i}B}^{\dagger}\alpha_{\mathbf{i}}, c_{\mathbf{i}\downarrow}^{\dagger} b_{\mathbf{i}\downarrow} \to \chi_{\mathbf{i}C}^{\dagger}\alpha_{\mathbf{i}}, \tag{19}$$

$$b_{\mathbf{i}\uparrow}^{\dagger} c_{\mathbf{i}\uparrow} \to \chi_{\mathbf{i}B}, b_{\mathbf{i}\uparrow}^{\dagger} c_{\mathbf{i}\downarrow} \to \chi_{\mathbf{i}C}, \tag{20}$$

$$b_{\mathbf{i}\downarrow}^{\dagger} c_{\mathbf{i}\uparrow} \to \alpha_i^{\dagger}\chi_{\mathbf{i}B}, b_{\mathbf{i}\downarrow}^{\dagger} c_{\mathbf{i}\downarrow} \to \alpha_{\mathbf{i}}^{\dagger}\chi_{\mathbf{i}C}, \tag{21}$$

and

$$f_{\mathbf{i}\uparrow}^{\dagger} b_{\mathbf{i}\uparrow} \to \chi_{\mathbf{i}D}^{\dagger}, f_{\mathbf{i}\downarrow}^{\dagger} b_{\mathbf{i}\uparrow} \to \chi_{\mathbf{i}F}^{\dagger}, \tag{22}$$

$$f_{\mathbf{i}\uparrow}^{\dagger} b_{\mathbf{i}\downarrow} \to \chi_{\mathbf{i}D}^{\dagger}\alpha_{\mathbf{i}}, f_{\mathbf{i}\downarrow}^{\dagger} b_{\mathbf{i}\downarrow} \to \chi_{\mathbf{i}F}^{\dagger}\alpha_{\mathbf{i}}, \tag{23}$$

$$b_{\mathbf{i}\uparrow}^{\dagger} f_{\mathbf{i}\uparrow} \to \chi_{\mathbf{i}D}, b_{\mathbf{i}\uparrow}^{\dagger} f_{\mathbf{i}\downarrow} \to \chi_{\mathbf{i}F}, \tag{24}$$

$$b_{\mathbf{i}\downarrow}^{\dagger} f_{\mathbf{i}\uparrow} \to \alpha_i^{\dagger}\chi_{\mathbf{i}D}, b_{\mathbf{i}\downarrow}^{\dagger} f_{\mathbf{i}\downarrow} \to \alpha_{\mathbf{i}}^{\dagger}\chi_{\mathbf{i}F}. \tag{25}$$

Here B, C, D, F denote $j_z = 1/2, j_z = -1/2, j_z = 3/2, j_z = -3/2$ quantum numbers, respectively.

(iii) We perform the Fourier and Bogolyubov transformations (see e.g. Ref. [28]):

$$\begin{aligned} a_{\mathbf{q}} &= u_{\mathbf{q}}\alpha_{\mathbf{q}} - v_{\mathbf{q}}\alpha_{-\mathbf{q}}^{\dagger}, \\ a_{-\mathbf{q}}^{\dagger} &= u_{-\mathbf{q}}\alpha_{-\mathbf{q}}^{\dagger} - v_{\mathbf{q}}\alpha_{\mathbf{q}} \end{aligned} \tag{26}$$

where the magnon energy $\omega_{\mathbf{q}} = \sqrt{A_{\mathbf{q}}^2 - B_{\mathbf{q}}^2}$ and Bogolyubov coefficients $u_{\mathbf{q}}$, $v_{\mathbf{q}}$ are given by the usual expressions in the linear spin-wave theory:

$$u_{\mathbf{q}} = \frac{1}{\sqrt{2}}\sqrt{\frac{A_{\mathbf{q}}}{\omega_{\mathbf{q}}} + 1}, v_{\mathbf{q}} = -\frac{sign(B_{\mathbf{q}})}{\sqrt{2}}\sqrt{\frac{A_{\mathbf{q}}}{\omega_{\mathbf{q}}} - 1}, \tag{27}$$

where the coefficients $A_{\mathbf{q}}$ and $B_{\mathbf{q}}$ are defined in a usual way, see e.g. Eq. (8) in the Supplementary Material of Ref. [14]. Here we neglected terms comprising two magnon operators, since it was shown that coupling to two magnons does not significantly change the polaronic spectrum (see for example Ref. [31]).

After applying the above transformations to the Hamiltonian (13) we arrive at the following polaronic Hamiltonian for the propagation of the $j_{\text{eff}} = 3/2$ spin-orbit exciton (see also main text of the paper):

$$H_{\text{JT}}^{exc} = \sum_{\mathbf{k},\mathbf{q}} [\hat{M}_{\mathbf{k},\mathbf{q}}^{\text{JT}} \hat{\chi}_{\mathbf{k}}^{\dagger} \hat{\chi}_{\mathbf{k}-\mathbf{q}} a_{\mathbf{q}} + h.c.] + \sum_{\mathbf{k}} \hat{E}_{\mathbf{k}}^{\text{JT}} \hat{\chi}_{\mathbf{k}}^{\dagger} \hat{\chi}_{\mathbf{k}}, \tag{28}$$

with the momentum-dependent vertices $\hat{M}_{\mathbf{k},\mathbf{q}}^{\text{JT}} = zV\hat{m}^{\text{JT}} \cdot |\gamma_{\mathbf{k}} v_{\mathbf{q}} + \gamma_{\mathbf{k}-\mathbf{q}} u_{\mathbf{q}}|/\sqrt{N}$ and $\hat{E}_{\mathbf{k}}^{\text{JT}} = zV\hat{e}^{\text{JT}} \cdot |\gamma_{\mathbf{k}}|$. Here $\gamma_{\mathbf{q}} = \frac{1}{2}\sum_{\mathbf{r}} \cos \mathbf{q} \cdot \mathbf{r}$ and the diagonal (off-diagonal) matrix $\hat{m}^{\text{JT}}$ ($\hat{e}^{\text{JT}}$) describes the polaronic (free) hopping reads:

$$\hat{m}^{\text{JT}} = \frac{1}{3}\begin{pmatrix} \frac{1}{3}+\frac{\kappa}{2} & 0 & 0 & 0 \\ 0 & \frac{1}{3}+\frac{\kappa}{2} & 0 & 0 \\ 0 & 0 & 1+\frac{\kappa}{2} & 0 \\ 0 & 0 & 0 & 1+\frac{\kappa}{2} \end{pmatrix}, \tag{29}$$

(30)

and

$$\hat{e}^{\text{JT}} = \frac{2}{3}\begin{pmatrix} 0 & -\frac{1}{3} & -\frac{\sqrt{3}\kappa}{2} & 0 \\ -\frac{1}{3} & 0 & 0 & -\frac{\sqrt{3}\kappa}{2} \\ -\frac{\sqrt{3}\kappa}{2} & 0 & 0 & -1+\kappa \\ 0 & -\frac{\sqrt{3}\kappa}{2} & -1+\kappa & 0 \end{pmatrix}, \tag{31}$$

which acts on the row of kets of the 'excited states' $X = (|j_z = 1/2\rangle, |j_z = -1/2\rangle, |j_z = 3/2\rangle, |j_z = -3/2\rangle)$ with $j_{\text{eff}} = 3/2$.

## B: dependence of the results on the model parameters

In this part of the supplemental materials we show how the spectral function of the spin-orbit exciton calculated within our model depends on the model parameters: the on-site spin-orbit coupling $\lambda$, the on-site energy gap between the $|j_z| = 1/2$ and $|j_z| = 3/2$ excitons (following the notation used in Ref. [14] we call it $\Delta_{BC}$ below), and the Jahn-Teller coupling constants $V$ and $\kappa$. [The results for different choices of the superexchange parameters can already be inferred from Refs. [13, 14].]

In Fig. 5(a) the excitonic spectrum is shown for the value of $\lambda = 6.67J_1$ (which corresponds to one of the proposed values of $\lambda = 400$ meV [10] for $Sr_2IrO_4$). We see that increasing the value of the spin-orbit coupling with respect to the one chosen in the main text of the paper leads to a merely modest shift of the spectral weight to higher energies without a significant change of the shape of the spectra. The decrease of the on-site energy gap between the $|j_z| = 1/2$ and $|j_z| = 3/2$ excitons from its main-text value of $\Delta_{BC} = 2.29J_1$ to $\Delta_{BC} = 1.86J_1$ (which follows from the crystal field splitting $\Delta = -155$ meV as suggested for $Sr_2IrO_4$ by e.g. Ref. [39]), cf. Fig. 5(b), leads to a small shift of the spectrum and also slightly renormalises the spectral weight, especially around $(\pi, 0)$.

In Fig. 5(c)-5(f) the dependence of the excitonic spectrum on the Jahn-Teller coupling constants is shown. Since the values of the Jahn-Teller coupling constants are rather hard to estimate and to the best of our knowledge no estimates are available for $Sr_2IrO_4$, we vary these

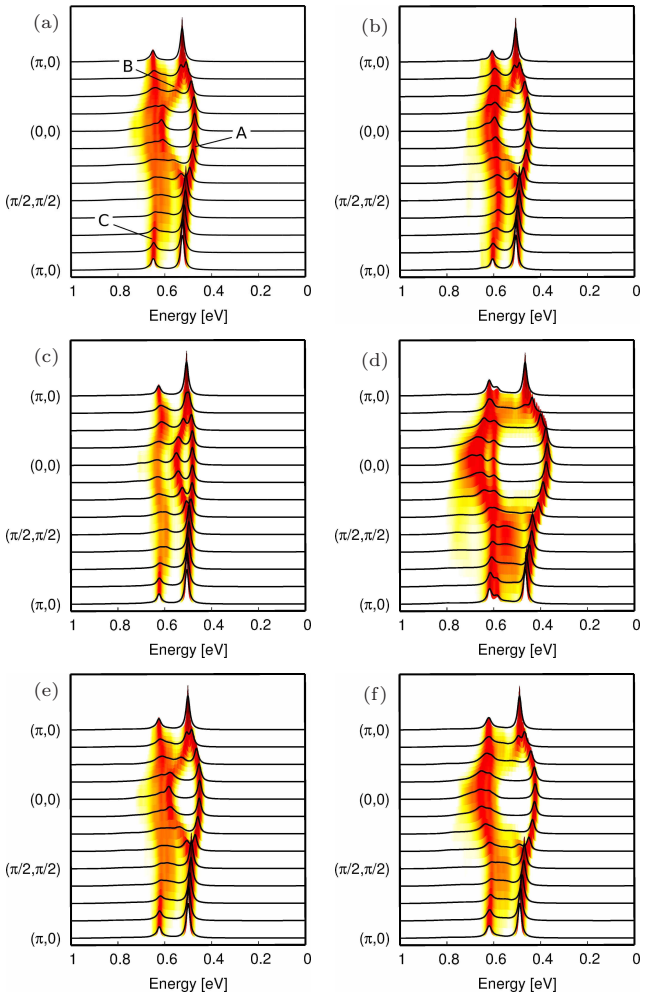


FIG. 5: Dependence of the spin-orbit exciton spectral function on the parameters of the model [Eq. (4) in the main text of the paper]: on-site spin-orbit coupling $\lambda$, the on-site energy gap between the $|j_z| = 1/2$ and $|j_z| = 3/2$ excitons $\Delta_{BC}$, and the Jahn-Teller coupling constant $V$ and $\kappa$: (a) $\lambda = 6.67J_1$, (b) $\Delta_{BC} = 1.86J_1$, (c) $V = 0.4J_1$, (d) $V = 1.6J_1$, (e) $\kappa = 0.025$, (f) $\kappa = 0.4$. If not specified above, all other model parameters are as in the main text of the paper (cf. caption of Fig. 2). Letters 'A', 'B', 'C' in panel (a) denote three main spectral features of the spectrum – see text for further details.

values in a rather wide range. First we take $V$ twice smaller than the one used in the main text of the paper, $V = 0.4J_1$, and keep $\kappa$ unchanged. As we see in Fig. 5(c) such change affects the spectra in the following way: the middle feature [denoted as 'B' in Fig. 5(a)] shifts to the lower energies, separates more from the the highest one [denoted as 'C' in Fig. 5(a)], and forms a clear maximum at the $\Gamma$ point. Next, if we make $V$ twice larger w.r.t. the value suggested in the main text of the paper [see Fig. 5(d)], then the effect is exactly opposite: feature B shifts to higher energies, almost merges with C and some spectral weight shifts from feature B to C. Finally, as

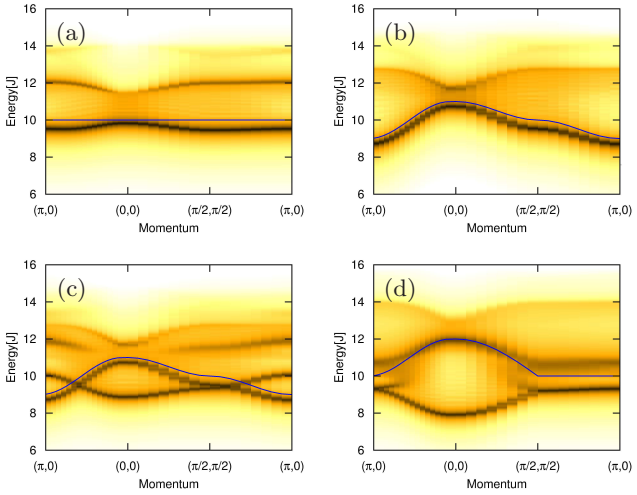


FIG. 6: Toy model illustrating the interplay between the polaronic hopping and the various types of the free excitonic hopping: (a) no free hopping, (b) diagonal free hopping of next-nearest-neighbor type, (c) off-diagonal free hopping of next-nearest-neighbor type, (d) off-diagonal free hopping of nearest-neighbor type; see text for further details. The solid line denotes the dispersion arising from pure free hopping (i.e. the polaronic hopping is not included).

one varies $\kappa$, one sees almost no changes for a smaller value of $\kappa$ w.r.t. the value suggested in the main text of the paper [see Fig. 5(e)], while for a relatively large $\kappa$ there is a relatively large shift of the spectral weight from feature B to C. It should also be noted that increasing the strength of the Jahn-Teller couplings (by making either $V$ *or* $\kappa$ larger) leads to a larger dispersion relation of all the features.

Altogether we conclude that there are rather severe constraints on the possible realistic values of these parameters, provided that the spectrum is intended to describe the excitonic propagation in one of the quasi-2D iridates (such as e.g. $Sr_2IrO_4$). Moreover, the changes in the excitonic spectrum, due to the small variations in $\lambda$ or $\Delta_{BC}$, are rather small. On the other hand, the values of the Jahn-Teller constants in the iridium oxides are rather hard to estimate and the large variations in the values of the Jahn-Teller constants may indeed lead to some more substantial changes in the shape of the excitonic spectrum. Nevertheless, such changes are never as substantial as to completely alter the main qualitative features of the excitonic spectrum: the mere existence of the three main features (A, B, C) as well as the generic features of their dispersion relations.

### C: Understanding the free excitonic hopping arising from the Jahn-Teller model

In order to better understand the interplay of polaronic and free hopping processes in the Jahn-Teller and superexchange models, we introduced a toy model which

is based on the above-written polaronic form of the Jahn-Teller model – though with modified polaronic and free hopping couplings in the following way:

First of all, we assume that the longer range exchange between the $j_{\rm eff} = 1/2$ magnons vanishes, i.e. $J_2 = J_3 = 0$. Secondly, we assume a diagonal form of the matrix describing the polaronic hopping: $\hat{m}^{\rm JT} \to \mathbb{I}$. Next, we consider four different forms of the free hopping processes:

In the first place, we put $\hat{E}^{\rm JT}_{\mathbf{k}} \to 0$ – the corresponding spectral function, calculated using SCBA (see main text of the paper), is shown in Fig. 6(a). It is interesting to note that adding a next-nearest-neighbor free excitonic hopping with only diagonal elements between different flavors of the excitons, i.e. substituting $\hat{E}^{\rm JT}_{\mathbf{k}} \to zV\mathbb{I}\cdot|\gamma_{2\mathbf{k}}|$ (where $\gamma_{2\mathbf{k}} = \cos k_x \cos k_y$), does not change the generic features of the spectral function a lot, see Fig. 6(b). Since the latter case qualitatively resembles the superexchange model for the excitonic hopping, as discussed in Ref. [14] and in the main text of the paper, this means that within the superexchange model the polaronic and the free hopping are responsible for the qualitatively similar features in the spectral function. This is because, in the superexchange case both the polaronic and the free hopping allow for an effectively next-nearest-neighbor type of the excitonic dispersion.

In the next step, we switch off the diagonal terms in the matrix describing the free excitonic hopping and instead introduce the off-diagonal free hopping – in order to mimic the Jahn-Teller model. More precisely, we substitute $\hat{E}^{\rm JT}_{\mathbf{k}} \to zV\mathbb{A}\cdot|\gamma_{2\mathbf{k}}|$, where matrix $\mathbb{A}$ has the form:

$$\mathbb{A} = \begin{pmatrix} 0 & 0 & 1 & 0 \\ 0 & 0 & 0 & 1 \\ 1 & 0 & 0 & 0 \\ 0 & 1 & 0 & 0 \end{pmatrix} \tag{32}$$

As one can easily see in Fig. 6(c), involving the non-diagonal elements in the free hopping matrix instead of the diagonal ones drastically changes the spectrum – in particular, each of the two dispersive branches splits now into two branches. Finally, the spectrum in Fig. 6(d) is calculated for a toy model which also has the off-diagonal free hopping elements in the matrix – however, instead of the next-nearest-neighbor hopping it includes solely the nearest-neighbor hopping [i.e. we substitute $\hat{E}^{\rm JT}_{\mathbf{k}} \to zV\mathbb{A}\cdot|\gamma_{\mathbf{k}}|$]. We note that the latter case of the toy model is the closest (out of all four toy models discussed) to the considered in the main text Jahn-Teller model.

One can see that the spectra in Figs. 6(c) and 6(d) have slightly more in common than the spectra in Figs. 6(b) and 6(c). This means that the presence of the off-diagonal hopping elements in the free excitonic hopping plays an even more important role in the propagation of the exciton, than the type of the free excitonic hopping dispersion (i.e. whether it is of the nearest- or next-nearest-neighbor character).

Altogether, we have shown that the particular features found in the excitonic spectrum of the Jahn-Teller model, which make it so different with respect to the superexchange model, originate from: (i) the nearest-neighbor-character of the free hopping that is always present in the Jahn-Teller Hamiltonian and has no analog in the superexchange model, and (ii) the off-diagonal elements in the free hopping matrix – which is also absent in the superexchange case.

* e.plotnikova@ifw-dresden.de


[1] M. Z. Hasan and C. L. Kane, Rev. Mod. Phys. **82**, 3045 (2010).
[2] X.-L. Qi and S.-C. Zhang, Rev. Mod. Phys. **83**, 1057 (2011).
[3] D. Pesin and L. Balents, Nature Physics **6**, 376 (2010).
[4] W. Witczak-Krempa, G. Chen, Y. B. Kim, and L. Balents, Annual Review of Condensed Matter Physics **5**, 57 (2014).
[5] E. J. Bergholtz and Z. Liu, International Journal of Modern Physics B **27**, 1330017 (2013).
[6] G. Jackeli and G. Khaliullin, Phys. Rev. Lett **102**, 017205 (2009).
[7] J. Chaloupka, G. Jackeli, and G. Khaliullin, Phys. Rev. Lett. **105**, 027204 (2010).
[8] A. Kitaev, Annals of Physics **321**, 2 (2006).
[9] G. Baskaran, S. Mandal, and R. Shankar, Phys. Rev. Lett. **98**, 247201 (2007).
[10] B. J. Kim *et al.*, Phys. Rev. Lett. **101**, 076402 (2008).
[11] F. Wang and T. Senthil, Phys. Rev. Lett. **106**, 136402 (2011).
[12] H. Watanabe, T. Shirakawa, and S. Yunoki, Phys. Rev. Lett. **110**, 027002 (2013).
[13] J. Kim *et al.*, Phys. Rev. Lett. **108**, 177003 (2012).
[14] J. Kim *et al.*, Nat. Commun. **5**, 4453 (2014).
[15] Y. K. Kim *et al.*, Science **345**, 187 (2014).
[16] Y. K. Kim, N. H. Sung, J. D. Denlinger, and B. J. Kim, Nat. Phys. (Advanced Online Publication) (2015).
[17] Y. J. Yan *et al.*, Phys. Rev. X **5**, 041018 (2015).
[18] J. Chaloupka, G. Jackeli, and G. Khaliullin, Phys. Rev. Lett. **110**, 097204 (2013).
[19] A. M. Oleś, G. Khaliullin, P. Horsch, and L. F. Feiner, Phys. Rev. B **72**, 214431 (2005).
[20] J. Kanamori, Journal of Applied Physics **31**, S14 (1960).
[21] K. I. Kugel' and D. I. Khomskii, Sov. Phys. Usp. **25**, 231 (1984).
[22] J. Nasu and S. Ishihara, Phys. Rev. B **88**, 094408 (2013).
[23] J. Nasu and S. Ishihara, Phys. Rev. B **91**, 045117 (2015).
[24] G. Khaliullin, Prog. of Theor. Phys. Suppl. **160**, 155 (2005).
[25] H. Gretarsson *et al.*, ArXiv e-prints: 1509.03396 (2015).
[26] K. Wohlfeld *et al.*, Physical Review Letters **107**, 147201 (2011).
[27] J. Schlappa *et al.*, Nature **485**, 82 (2012).
[28] G. Martinez and P. Horsch, Phys. Rev. B **44**, 317 (1991).
[29] C. L. Kane, P. A. Lee, and N. Read, Phys. Rev. B **39**, 6880 (1989).

[30] K. Wohlfeld, A. M. Oleś, and P. Horsch, Phys. Rev. B **79**, 224433 (2009).
[31] J. Bala, A. M. Oleś, and J. Zaanen, Phys. Rev. B **52**, 4597 (1995).
[32] See Supplemental Materials at ... for details.
[33] L. J. P. Ament, G. Khaliullin, and J. van den Brink, Phys. Rev. B **84**, R020403 (2011).
[34] C. Jia *et al.*, ArXiv e-prints: 1510.05068 (2015).
[35] H. Gretarsson *et al.*, Phys. Rev. Lett. **110**, 076402 (2013).
[36] D. Feinberg, P. Germain, M. Grilli, and G. Seibold, Phys. Rev. B **57**, R5583 (1998).
[37] L. F. Feiner and A. M. Oleś, Phys. Rev. B **59**, 3295 (1999).
[38] W. Brzezicki, A. M. Oleś, and M. Cuoco, Phys. Rev. X **5**, 011037 (2015).
[39] N. A. Bogdanov *et al.*, Nat. Commun. **6**, 7306 (2015).